

A Family of Recompositions of the Penrose Aperiodic Protoset and its Dynamic Properties

Vivian Olsiewski Healey
University of Notre Dame, vhealey@math.brown.edu

Follow this and additional works at: <https://scholar.rose-hulman.edu/rhumj>

Recommended Citation

Healey, Vivian Olsiewski (2011) "A Family of Recompositions of the Penrose Aperiodic Protoset and its Dynamic Properties," *Rose-Hulman Undergraduate Mathematics Journal*: Vol. 12 : Iss. 2 , Article 7.
Available at: <https://scholar.rose-hulman.edu/rhumj/vol12/iss2/7>

ROSE-
HULMAN
UNDERGRADUATE
MATHEMATICS
JOURNAL

A FAMILY OF RECOMPOSITIONS OF THE
PENROSE APERIODIC PROTOSET AND
ITS DYNAMIC PROPERTIES

Vivian Olsiewski Healey^a

VOLUME 12, No. 2, FALL 2011

Sponsored by

Rose-Hulman Institute of Technology

Department of Mathematics

Terre Haute, IN 47803

Email: mathjournal@rose-hulman.edu

<http://www.rose-hulman.edu/mathjournal>

^aUniversity of Notre Dame

A FAMILY OF RECOMPOSITIONS OF THE PENROSE
APERIODIC PROTOSET AND ITS DYNAMIC
PROPERTIES

Vivian Olsiewski Healey

Abstract. This paper examines a recomposition of the rhombic Penrose aperiodic protoset due to Robert Ammann. We show that the three prototiles that result from the recomposition form an aperiodic protoset in their own right without adjacency rules and that every tiling admitted by this protoset (here called an Ammann tiling) is mutually locally derivable with a Penrose tiling. Although these Ammann tilings are not self-similar, an iteration process inspired by Penrose composition is defined on the set of Ammann tilings that produces a new Ammann tiling from an existing one, and the exact relationship to Penrose composition is examined. Furthermore, by characterizing each Ammann tiling based on a corresponding Penrose tiling and the location of the added vertex that defines the recomposition process, we show that repeated Ammann iteration proceeds to a limit for the local geometry.

1 Introduction

The Penrose aperiodic tiles have been well-studied by deBruijn [2], Lunnon and Pleasants [4], and others. See Senechal [7] for a survey. This paper describes a recomposition attributed to Robert Ammann of the rhombic Penrose aperiodic protoset P3 [3]. We give a proof that the three tiles that result from the construction form an aperiodic protoset in their own right without adjacency rules, a result that was previously known but never proven in the literature. We then define an iteration process on the space of Ammann tilings inspired by Penrose composition and show that this process proceeds to a limit for the local geometry.

While there are a variety of tilings attributed to Roger Penrose, the kind relevant to this paper are those admitted by a protoset of two rhombic tiles, a thin and a thick, with dimensions dependent on the golden ratio $\phi = \frac{1+\sqrt{5}}{2}$. This set of two tiles, referred to as P3, can be used to tile the plane non-periodically (without translational symmetry) when assembled following specific adjacency rules (see Figure 1(a)).

An Ammann tiling (see Figure 1(b)) may be constructed from a Penrose tiling by rhombs via a process called *recomposition*. In this particular construction, a single vertex Q is added within a thin Penrose rhomb, and edges are drawn between it and the three nearest Penrose vertices. The geometry of the newly constructed edges are then used to create two specific new vertices and five new edges inside the thick Penrose rhomb. These new vertices and edges are then copied into every Penrose rhomb in the tiling, and the original Penrose edges are deleted.

This construction of Ammann tilings from Penrose tilings is given in Branko Grünbaum and G.C. Shephard's *Tilings and Patterns* [3] but has never been thoroughly studied in the literature to the knowledge of this author. The construction is attributed to Robert Ammann, which is why we refer to the resulting tilings as "Ammann tilings." However, there are already a number of other tilings with this label in the literature, so the tilings in this paper should not be confused with any of these others. In [3] the authors note without proof that the resulting Ammann tiles form an aperiodic protoset without need of any additional adjacency rules. This protoset is a rare example of a protoset that contains very few tiles (in this case only three) all of which are convex and which admit only non-periodic tilings without added adjacency rules. After defining Ammann tilings independently of the recomposition process, we show that each Ammann tiling is mutually locally derivable with a Penrose tiling, and we use this result to prove the statement from [3] that the Ammann protosets are aperiodic. Although it is not discussed in further detail here, it should be noted that mutual local derivability is a significant result in its own right because it implies that the translation dynamical systems associated to the tilings are topologically conjugate (see [6] and [5] for this result and [8] for a description of the metric given to the tiling space).

We next describe an iteration process for Ammann tilings that resembles Penrose composition, the process of amalgamating certain tiles in a Penrose tiling to form a new Penrose tiling with tiles scaled by the golden ratio (Penrose tilings by half-rhombs have the unique composition property [9]). Ammann tilings are not self-similar and do not have the unique composition property, but we prove that the iteration process runs in parallel to Penrose

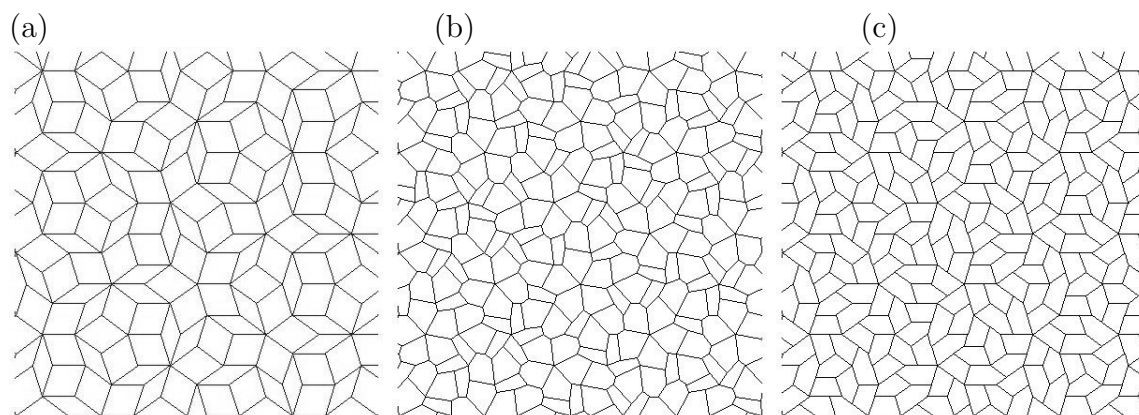


Figure 1: From left to right: a patch of a Penrose tiling, the corresponding patch of a generic Ammann tiling, a patch of an Ammann tiling with limiting prototiles.

composition.

In analyzing the Ammann iteration process further, we address the questions: (1) Is the iterated tiling composed of tiles geometrically similar to those of the original Ammann tiling? (2) If not, is there a sense in which the new tiling is of the same type as the original Ammann tiling? (3) Can this process be carried out using the new tiling as the starting point? and (4) If so, does the sequence of iterated tilings yield limiting shapes for the prototiles?

We show that the answers to questions (2), (3), and (4) are affirmative. The Ammann iteration process yields a limit for the local geometry of the tilings (see Figure 1 (c)) and the limiting shapes are explicitly determined. By identifying an Ammann tiling by two parameters (a) its corresponding Penrose tiling and (b) the location of the added vertex Q within a thin rhomb, we show that (b) approaches a limit. This result is summarized in the following theorem.

Theorem 1.1. *The map $Q \mapsto Q'$ defined by Ammann iteration has a unique attractive fixed point along the edge of the thin Penrose rhomb which divides that edge according to the golden ratio.*

Section 2 reviews the necessary terminology related to tilings, and Section 3 summarizes the relevant properties of Penrose tilings. Section 4 describes Ammann tilings, detailing the recomposition process that constructs an Ammann tiling from a Penrose tiling. It goes on to prove that Penrose and Ammann tilings are mutually locally derivable and thus that the three tiles that result from the recomposition process form an aperiodic protoset. Section 5 describes the iteration process for Ammann tilings and shows the correspondence between Ammann iteration and Penrose composition. In section 6, we examine the dynamics of the Ammann iteration process and prove Theorem 1.1.

The research for this paper was begun at the National Science Foundation sponsored Research Experience for Undergraduates at Canisius College under the guidance of Professors Terry Bisson and B.J. Kahng. The project was continued at the University of Notre Dame

with Professor Arlo Caine and was funded with the help of Professor Frank Connolly through NSF Grant DMS-0601234. Many thanks to Professor Caine for the long hours he spent with me on this project and in particular for a suggestion that simplified the proof of Theorem 6.1. Without his help this project would not have been possible. Also, thanks to Professor Jeffrey Diller for suggestions pertaining to the dynamics of the Ammann iteration process.

2 Terminology

A *plane tiling* is a countable family $\mathcal{T} = \{T_1, T_2, \dots\}$ of closed subsets of the Euclidean plane, each homeomorphic to a closed circular disk, such that the union of the sets T_1, T_2, \dots (which are known as the *tiles* of \mathcal{T}) is the whole plane, and the interiors of the sets T_i are pairwise disjoint [3]. We say that a set \mathcal{S} of representatives of the congruence classes in \mathcal{T} is a *protoset* for \mathcal{T} , and each representative is a *prototile*. If \mathcal{S} is a protoset for \mathcal{T} , then we say that \mathcal{S} *admits* \mathcal{T} .

A *patch* is a finite set of tiles whose union is simply connected. A patch is called *locally legal* if the tiles are assembled according to the relevant adjacency rules and is called *globally legal* if it can be extended to an infinite tiling.

The (*first*) *corona* of a tile T_i is the set

$$\mathcal{C}(T_i) = \{T_j \in \mathcal{T} : \exists x, y \in T_i \cap T_j \text{ such that } x \neq y\}.$$

The (*first*) *corona atlas* is the set of all (first) coronas that occur in \mathcal{T} , and a *reduced (first) corona atlas* of \mathcal{T} is a subset of the corona atlas of \mathcal{T} that covers \mathcal{T} . Similarly, the (*first*) *vertex star* of a vertex v is the set $\mathcal{V}(v) = \{T_j \in \mathcal{T} \mid T_j \cap \{v\} \neq \emptyset\}$, and a (*first*) *vertex star atlas* is the set of all (first) vertex stars that occur in \mathcal{T} . A tiling \mathcal{T} in \mathbb{R}^2 is *nonperiodic* if it does not have translational symmetry, and a set of prototiles \mathcal{S} is *aperiodic* if it admits only nonperiodic tilings.

A tiling \mathcal{T} is *self-similar* if the tiling can be dilated so that each resulting tile can be decomposed exactly into a configuration of tiles congruent to the originals. (For example, when the Penrose rhombs are split in half as in Figure 2, the resulting tiling by triangles is self-similar.) A tiling has the *unique composition property* if its tiles may be amalgamated in a uniquely defined way to form a new tiling with tiles geometrically similar to the originals. (Solomyak shows in [9] that nonperiodic translationally finite self-similar tilings always have the unique composition property.)

A tiling \mathcal{T}' is said to be *locally derivable* from a tiling \mathcal{T} if there is a translation and rotation invariant rule that recovers the tiles of \mathcal{T}' from a neighborhood of \mathcal{T} of a fixed radius (see [5]).

If \mathcal{T} is also locally derivable from \mathcal{T}' , then \mathcal{T} and \mathcal{T}' are said to be *mutually locally derivable*.

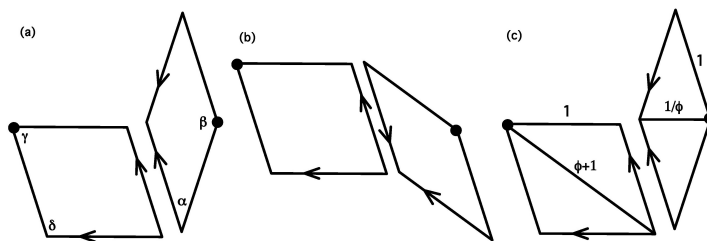


Figure 2: (a) the Penrose rhombs properly assembled, (b) the Penrose rhombs improperly assembled, (c) the Penrose rhombs split into triangles.

3 Penrose Tilings

There are several types of tilings known as Penrose tilings. The type relevant to this paper is built from the two rhombic prototiles shown in Figure 2(a). The sides of the rhombs are all of length one and the angles measure $\alpha = \frac{\pi}{5}$, $\beta = \frac{4\pi}{5}$, $\gamma = \frac{2\pi}{5}$, and $\delta = \frac{3\pi}{5}$. In order to guarantee a non-periodic tiling, the edge and angle markings must line up with each other as in Figure 2(a). Illegal configurations, such as the one in Figure 2(b), either produce a periodic tiling of the plane or prevent a tiling of the plane.

It is well known that the Penrose rhombs, together with the adjacency rules, form an aperiodic protoset and that the Penrose protoset admits uncountably many noncongruent tilings of the plane (as all aperiodic protosets do) [7]. The rhombic prototiles may equivalently be thought of as pairs of triangles, as shown in Figure 2(c), the smaller with side lengths 1 and $\frac{1}{\phi}$, where ϕ is the golden ratio $\phi = \frac{1+\sqrt{5}}{2} = 1.618\dots$, and the larger with side lengths 1 and $\phi+1$ (see Figure 2). Penrose tilings by triangles are self-similar and possess the unique composition property [3], [9]. Considering the Penrose rhombs as pairs of triangles, we can perform the uniquely defined composition process to get another Penrose tiling by pairs of triangles that can be amalgamated into rhombs. The resulting tiling is called the *inflated Penrose tiling*. When considering the space of Penrose tilings \mathbb{P} equipped with the metric defined in [8], composition is homeomorphism from \mathbb{P} to itself.

4 Ammann Tilings and Their Combinatorial and Geometric Properties

Ammann tilings are derived from Penrose tilings by extending the local map $\hat{\mathcal{C}}_Q$ described below to all patches in the tiling. (See [6] for more on this method). This process gives a local rule for constructing an Ammann tiling from a Penrose tiling. Thus, by definition these Ammann tilings are locally derivable from Penrose tilings.

We will give a definition of of Ammann tilings that is independent of the recomposition construction and then prove that each Ammann tilings is mutually locally derivable with a Penrose tiling. From this result we conclude that the Ammann protoset is aperiodic. (It

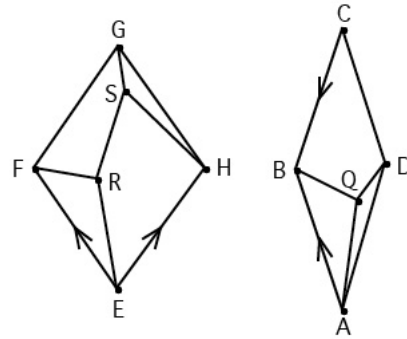


Figure 3: The recombination of Penrose thick and thin rhombs into Ammann tiles.

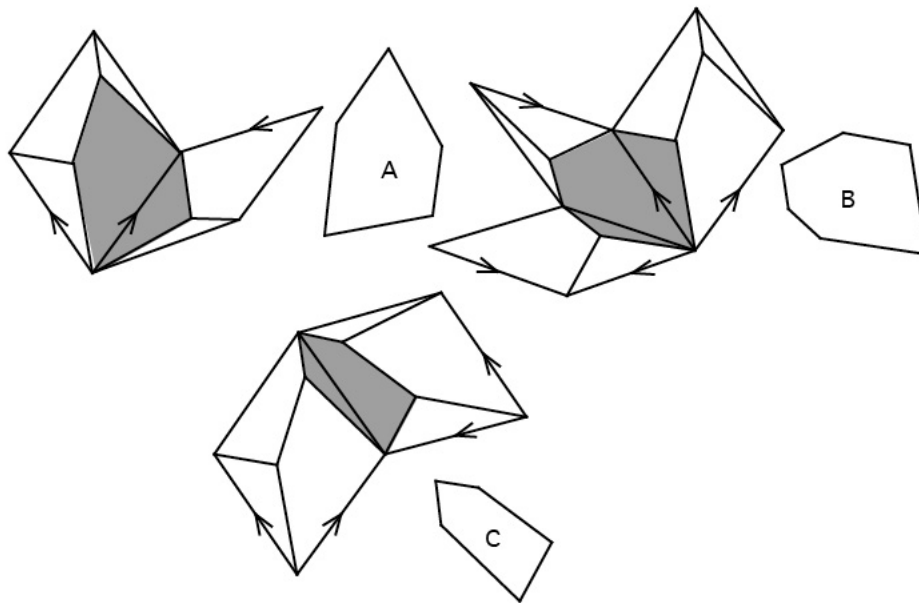


Figure 4: The Ammann tiles created from recombination.

should be noted that another straightforward way to prove that a protoset is aperiodic is to show the stronger condition that the tilings it admits have the unique composition property, as in [1]. However, Ammann tilings do not have the unique composition property, so this method of proof is not at our disposal.)

Recomposition 4.1. *Figure 3 illustrates this construction. Let \mathcal{P}_i be a patch in a Penrose tiling \mathcal{P} . Let Q be a point within a single thin rhomb of \mathcal{P}_i . Without loss of generality, we assume Q is in the lower half of the rhomb. Then the following construction defines the map $\hat{\mathcal{C}}_Q : \mathcal{P}_i \rightarrow \mathcal{T}_{Q,i}$, where $\mathcal{T}_{Q,i}$ is an Ammann patch.*

1. Construct edges connecting Q to the three closest vertices of the rhomb.
2. Copy this construction into all thin rhombs in \mathcal{P}_i .
3. Copy $\triangle ABQ$ into the lower left of each thick rhomb such that $\overrightarrow{AB} \mapsto \overrightarrow{EF}$ and a new point is created $Q \mapsto R$ to yield $\triangle EFR$ within the thick rhomb.
4. Copy $\triangle DAQ$ into the upper right of each thick rhomb in \mathcal{P}_i such that $\overrightarrow{DA} \mapsto \overrightarrow{GH}$ and a new point is created $Q \mapsto S$ to yield $\triangle GHS$ within each thick rhomb.
5. Construct an edge connecting points R and S within every thick rhomb.
6. Erase the edges of the tiles of \mathcal{P}_i .

Note that Q may be chosen on the boundary of the thin rhomb, but in this degenerate case we need to regard the resulting Ammann tiling as having two edges that meet at Q at an angle of π , rather than thinking of them as a single edge. This ensures that we abide by our convention that adjacent tiles must share a complete edge. This degenerate case turns out to be even more interesting than the general case, as we will see in Theorem 6.1.

Since \mathcal{P} is covered by a countable number of patches \mathcal{P}_i , and $\hat{\mathcal{C}}_Q$ is well defined when the patches overlap (since it is defined on the individual tiles), we can extend $\hat{\mathcal{C}}_Q$ to a map $\mathcal{C}_Q : \mathcal{P} \rightarrow \mathcal{T}_Q$ as in [6] ‘by concatenation,’ that is, by applying $\hat{\mathcal{C}}_Q$ to each patch of \mathcal{P} .

We will call a choice of Q allowable if no two of the lengths $|AQ|$, $|BQ|$, $|CQ|$, $|RS|$ are equal. Our proofs apply only to allowable choices of Q , since equality among two or more of these edge lengths would increase the number of locally legal configurations of the three resulting Ammann prototiles.

Proposition 4.2. *Let \mathcal{P} be a Penrose tiling. Let $\mathcal{T}_Q = \mathcal{C}_Q(\mathcal{P})$. \mathcal{P} and \mathcal{T}_Q are mutually locally derivable.*

Proof. Instead of considering how \mathcal{C}_Q acts on arbitrary patches of a Penrose tiling, it is sufficient to examine how it acts on the globally legal Penrose vertex stars, since they exhaust all possible configurations within a Penrose tiling. Examining Figure 5, we see that when the tiles of Penrose tiling \mathcal{P} are overlaid on the tiles of $\mathcal{T}_Q = \mathcal{C}_Q(\mathcal{P})$, the edges of \mathcal{P} always cut each tile of \mathcal{T} in a specific way determined by its Ammann type, as shown in Figure 6.

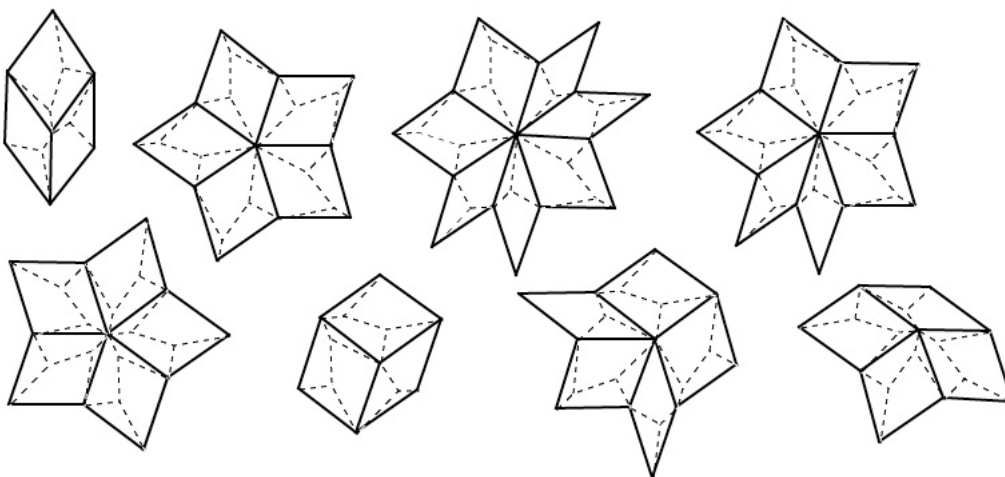


Figure 5: The eight globally legal Penrose vertex stars ([7], p177).

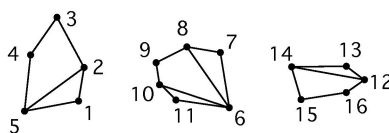


Figure 6: Divisions of Ammann tiles by Penrose rhombs of corresponding Penrose tiling \mathcal{P} .

Specifically, each type A tile of \mathcal{T} is cut once by segment $\overline{2,5}$, B tiles are cut twice by segments $\overline{8,6}$ and $\overline{10,6}$, and C tiles are cut once by segment $\overline{12,14}$. This implies that we can recover the original Penrose tiling \mathcal{P} from $\mathcal{T}_Q = \mathcal{C}_Q(\mathcal{P})$ by constructing edges $\overline{2,5}$, $\overline{8,6}$, $\overline{10,6}$, and $\overline{12,14}$ and eliminating the edges of the Ammann tiles. Thus, this process defines an inverse \mathcal{C}_Q^{-1} for \mathcal{C}_Q , so \mathcal{P} and \mathcal{T}_Q are mutually locally derivable. \square

Proposition 4.3. *Let $\mathcal{T}_Q = \mathcal{C}_Q(\mathcal{P})$, where \mathcal{P} is a Penrose tiling and Q is allowable, and let $\{A, B, C\}$ be the protoset that admits T_Q . Then following the labeling in Figures 7 and 8, the following edge and angle relations hold for $\{A, B, C\}$.*

1. $\varepsilon = \gamma = \nu = 2\theta$
2. $\iota = \lambda = 4\theta$
3. $\beta + \sigma = 6\theta$
4. $\chi + \rho + \omega = 10\theta$
5. $\delta + \tau + \eta = 10\theta$
6. $\alpha + \kappa + \mu = 10\theta$
7. $\alpha = \eta$

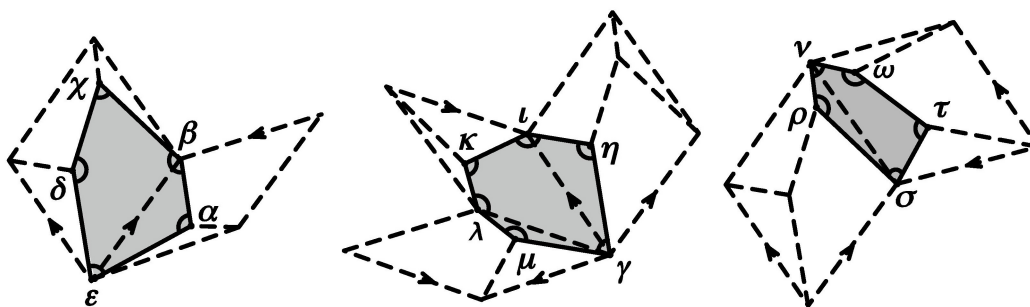


Figure 7:

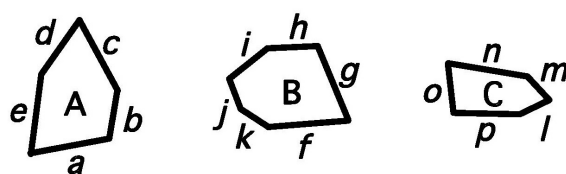


Figure 8:

- 8. $\mu = \rho$.
- 9. $a = c = e = f = g = n$
- 10. $b = h = i = o$
- 11. $j = k = l = m$
- 12. $d = p$

Proof. Since the thick rhombs have angles of $\frac{2}{5}\pi$ and $\frac{3}{5}\pi$, and the thin rhombs have angles of $\frac{1}{5}\pi$ and $\frac{4}{5}\pi$, we see in Figure 9 that

$$1. A + \Xi = \Theta + I = \frac{2}{5}\pi = 2\theta$$

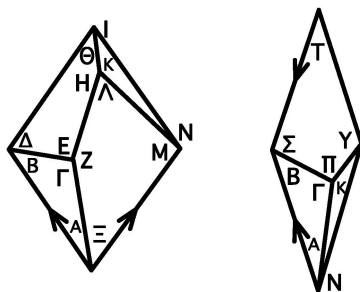


Figure 9:

$$2. B + \Delta = N + M = \frac{3}{5}\pi = 3\theta$$

$$3. A + N = T = \frac{1}{5}\pi = \theta$$

$$4. B + \Sigma = Y + I = \frac{4}{5}\pi = 4\theta.$$

Furthermore, we can see from Figure 7 and Figure 9 that $\alpha = \Gamma$, $\beta = B + M$, $\chi = \Lambda$, $\delta = Z$, $\varepsilon = \Xi + A = \gamma = A + T + N$, $\eta = \Gamma$, $\iota = B + \Sigma$, $\kappa = \Pi$, $\lambda = Y + I$, $\mu = K$, $\nu = \Theta + I$, $\rho = K$, $\sigma = \Delta + N$, $\tau = E$, $\omega = H$. It is easy to verify that these relations give us the desired result.

Finally, the edge congruences are evident by inspection of Figures 8 and 7. \square

Definition 4.4. *Using the edge labeling of Figure 8 and the angle labeling of Figure 7, we define an Ammann tiling to be a tiling of the plane admitted by a protoset of three tiles, two pentagons and a hexagon, satisfying the edge and angle relations of Proposition 4.3.*

Since these edge and angle relations are exhaustive, they exactly determine the locally legal configurations of tiles, so they determine the vertex star atlas of Ammann types. This vertex star atlas clearly contains the Ammann vertex stars that correspond to the eight globally legal Penrose vertex stars (these were the configurations we examined to arrive at the edge and angle relations). Thus, given an Ammann protoset $\{A, B, C\}$ and a Penrose tiling \mathcal{P} , $\{A, B, C\}$ admits a tiling \mathcal{T}_Q such that $\mathcal{T}_Q = \mathcal{C}_Q(\mathcal{P})$.

The next theorem says that in fact these are the only tilings that $\{A, B, C\}$ admits.

Theorem 4.5. *Let \mathcal{T}' be an arbitrary Ammann tiling. Then $\mathcal{T}' = \mathcal{C}_Q(\mathcal{P}')$ for some Q and some Penrose tiling \mathcal{P}' .*

In this case, we say that \mathcal{P}' is the *underlying Penrose tiling* of \mathcal{T}' .

Proof. Let \mathcal{T} be an Ammann tiling admitted by the same protoset as \mathcal{T}' , but with the additional assumption that $\mathcal{T} = \mathcal{C}_Q(\mathcal{P})$ for some Penrose tiling \mathcal{P} . We know that such a tiling exists by the discussion that precedes the statement of the theorem.

Because the Ammann vertex star atlas determines all Ammann tilings, and the Penrose vertex star atlas determines all Penrose tilings [7], it is sufficient to show that all possible vertex stars of \mathcal{T}' are derived from globally legal Penrose patches, i.e. that the vertex star atlas of \mathcal{T}' contains no configurations that are not in the vertex star atlas of \mathcal{T} .

Figure 10 shows eight possible Ammann vertex stars in the vertex star atlas of \mathcal{T}' . We see from Figure 5 that these eight correspond to the Penrose vertex star atlas, so they are globally legal and contained in the vertex star atlas of \mathcal{T} .

The recomposition process added the three vertices Q , R , and S , so we now consider their possible vertex stars. The five coronas of A shown in Figure 11 give us six more globally legal vertex stars shown in Figure 11. These were also constructed from the recomposition of a Penrose tiling, so they are globally legal and contained in the vertex star atlas of \mathcal{T} as well. This gives us fourteen globally legal vertex stars that may be in the vertex star atlas of \mathcal{T}' , all of which appear in the vertex star atlas of \mathcal{T} .

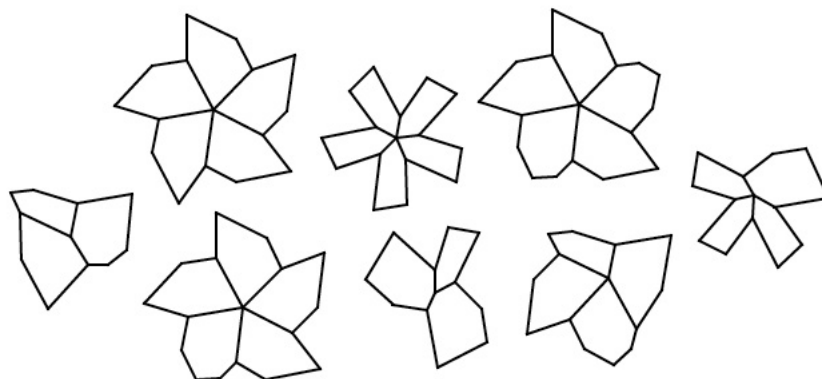


Figure 10: The eight Ammann vertex stars derived from the eight Penrose vertex stars in Figure 5.

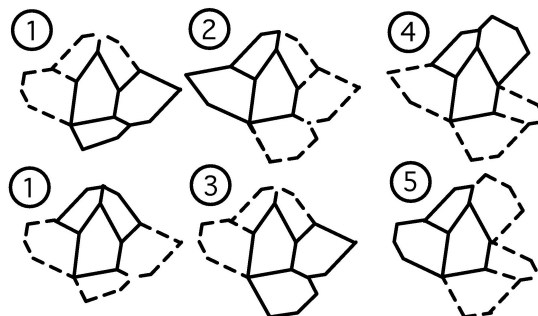


Figure 11: Six globally legal vertex stars obtained from the five coronas of a type *A* tile.

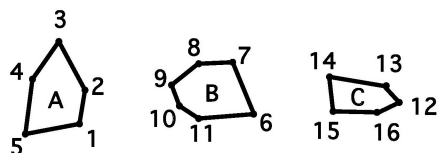


Figure 12:

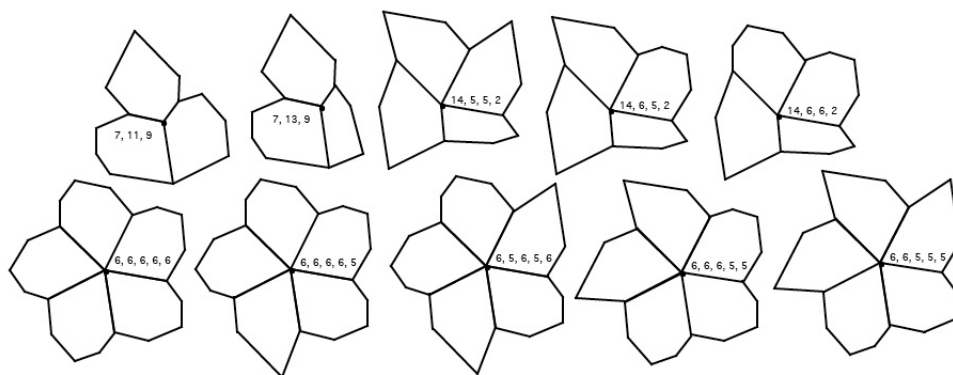


Figure 13:

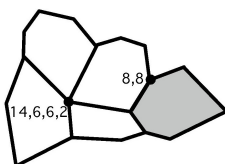


Figure 14:

Next, we use the angle and edge relations established in Proposition 4.3 to determine the other possible locally legal Amman vertex stars that could appear in \mathcal{T}' . We find that the only possibilities are the ten shown in Figure 13. (This is where we use the condition that the segments constructed in Algorithm 4.1 are of different lengths, i.e., that Q was allowable. If any were instead the same length, there would be more locally legal vertex stars than those shown here.) The central vertex of each vertex star in Figure 13 is labeled with the numbers of the vertices that meet there following the numbering in Figure 12.

Claim 4.6. *None of the ten vertex configurations in Figure 13 are globally legal.*

Notice that (7,13,9) and (7,11,9) are not globally legal because whenever vertices 7 and 9 meet, a space is created that cannot be filled (see Figure 15). Furthermore, when two instances of vertex 6 meet, vertices 7 and 11 also meet. But if vertices 7 and 11 meet, then

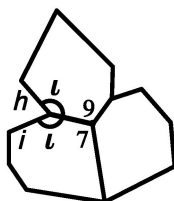


Figure 15: No tile has two adjacent sides of length $i = h$ and angle between them of $10\theta - 2\iota = 2\theta$, so the empty triangle on the left can never be filled.

vertex 9 meets there as well, because $\eta + \mu = 10\theta - \kappa$. However, as stated above, (7,11,9) is not globally legal, so a vertex star where two instances of vertex 6 meet is not globally legal. Therefore, (6,6,6,6,6), (6,6,6,6,5), (6,6,6,5,5), (6,6,5,5,5), (6,5,6,5,6), and (2,14,6,6) are not globally legal.

Now, we focus our attention to vertex stars (14,6,5,2) and (14,6,6,2). In both cases, only a B tile can fit adjacent to the C and B tiles on the right side of the vertex stars (see Figure 14) because the angle between them is $10\theta - \nu - \rho = \kappa$ and the edge lengths are m and h . This creates vertex (8,8) in which a tile would fit with a vertex angle of 2θ between congruent edges of length $h = i = b = o$. Since no such tile exists, the vertex star (8,8) cannot be completed, so vertex stars (14,6,5,2) and (14,6,6,2) are not globally legal. Finally, the left side of vertex star (14,5,5,2) contains vertex (3,4). Two edges of length d meet there at an angle of $10\theta - \chi - \delta$. Since no tile fits in this space, the vertex star is not globally legal. This proves the claim.

Therefore, all possible vertex stars in the the vertex star atlas of \mathcal{T}' are derived from Penrose tilings and so are in the vertex star atlas of \mathcal{T} , which is sufficient to prove the theorem. □

Corollary 4.7. *Each Ammann protoset is aperiodic.*

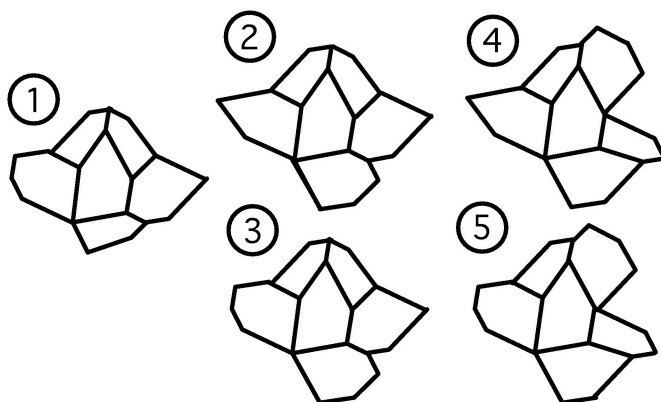
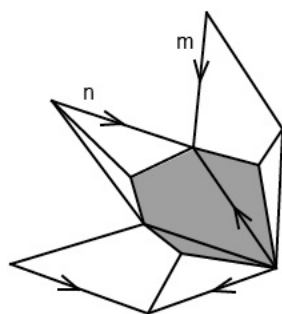
Proof. Since Penrose tilings are non-periodic, any tilings mutually locally derivable from Penrose tilings are also non-periodic. Theorem 4.5 and Proposition 4.2 together imply that every Ammann tiling \mathcal{T} is mutually locally derivable with a Penrose tiling. □

5 Iterating Ammann Tilings

Clearly Ammann tilings do not have the unique composition property, but this property motivates the following similar construction that builds Ammann tilings with larger and larger tiles from existing Ammann tilings. We will refer to this process as *Ammann iteration*. Iteration will be defined only on carefully chosen patches, but this construction can be extended to a map of the whole tiling if these patches cover the tiling and the map is still well defined where the patches overlap, as discussed in Section 4. In order to determine which patches we should choose to define the iteration map, we have the following two lemmas.

Lemma 5.1. *Given an Ammann tiling \mathcal{T} with underlying Penrose tiling \mathcal{P} , the five coronas illustrated in Figure 16 are the only possible coronas of an A tile of \mathcal{T} .*

Proof. (Sketch) As can be seen by inspection of Figure 4, there is a bijective correspondence between thick rhombs in \mathcal{P} and type A tiles in \mathcal{T} . So, to determine the possible coronas of A , we consider the possible Penrose coronas of a thick rhomb. The possible coronas of a Penrose thick rhomb are determined by the Penrose vertex atlas, and by applying \mathcal{C}_Q to the tiles of these Penrose coronas it can be seen that these five are the only possible coronas of an Ammann type A tile. □

Figure 16: The five coronas of an Ammann A tile.Figure 17: A locally legal construction of a B tile that is not globally legal.

Lemma 5.2. *The set of Ammann coronas of A is a reduced corona atlas.*

Proof. As in the previous theorem, let \mathcal{P} be the underlying Penrose tiling of an Ammann tiling \mathcal{T} . Assume for contradiction that the set of coronas of A does not cover \mathcal{T} . Then, there is at least one corona of a B or C tile that does not contain any A tiles.

By inspection of Figure 4, we can see that a thick rhomb is needed to create a C tile, so every C tile has an A tile in its corona. On the other hand, the patch shown in Figure 17 shows that it is locally legal to assemble three thin rhombs with Ammann markings to form a B tile. However, this configuration is not globally legal, as is immediately apparent when we try to put another tile between lines m and n . So, this configuration is impossible, and this set of five coronas of type A tiles covers \mathcal{T} , and is thus a reduced corona atlas. \square

Ammann Iteration 5.3. *Let \mathcal{T} be an Ammann tiling. Using Lemmas 5.1 and 5.2, defining Ammann iteration on the five coronas is sufficient to define it on an entire tiling. By constructing edges within the five coronas of A as shown in Figure 18 and then erasing the original edges, we create a new tiling of the plane.*

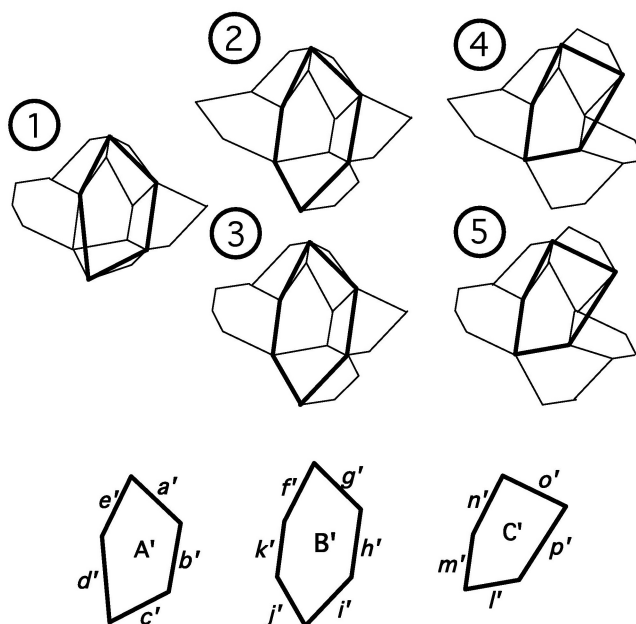


Figure 18: Algorithm 5.3 creates the three tiles of \mathcal{T}' from the coronas of A in \mathcal{T} . Note that if the tiles were rescaled by a factor of $\frac{1}{\phi}$ the new tiles would be similar in size to the originals.

Examining all possible arrangements of the five coronas, it is straightforward to check that this process is well defined on the overlaps of the coronas of A -tiles in an arbitrary Ammann tiling. Thus, iteration can be extended to the entire tiling, producing a tiling by the three prototiles shown in Figure 18. We label the new tiling \mathcal{T}' and call the new tiles from corona 1 the type A' tiles of \mathcal{T}' , the tiles from coronas 2 and 3 we call the type B' tiles, and the tiles from coronas 4 and 5 we call the type C' tiles. The angles and edges of the tiles of \mathcal{T}' are labeled in reverse, *i.e.* if the tiles of \mathcal{T} are labeled counter-clockwise, then those of \mathcal{T}' are labeled clockwise.

Theorem 5.4. *Let \mathcal{T} be an Ammann tiling. The tiling \mathcal{T}' obtained via Algorithm 5.3 is also an Ammann tiling.*

Proof. In order to prove this we need only refer back to Definition 4.4 that specified the angle and edge relations necessary for an Ammann protoset. By construction, as shown in Figure 18 the tiles in \mathcal{T}' obey

1. $a' = c' = e' = f' = g' = n'$
2. $b' = h' = i' = o'$
3. $k' = m'$.

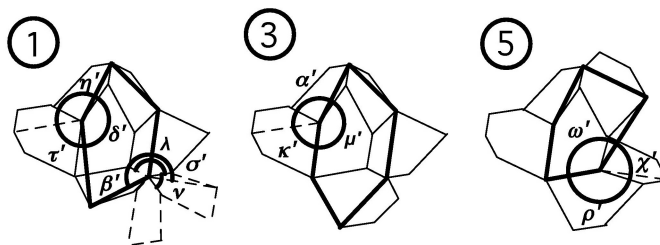


Figure 19:

Since in \mathcal{T} , $a = e = g$, we have $j' = k' = m' = l'$. Also, it can be easily shown that only an A tile would fit between the C and B tiles on the far right in corona 5 in Figure 19. This yields the edge length equality $d' = p'$. Therefore, we get the the fourth relation in Proposition 4.3 required of the edges in an Ammann protoset. So, the algorithm preserves the edge congruence relations.

By examining Figure 18, it is clear that the angles of \mathcal{T} are not congruent to the angles of \mathcal{T}' . However, we aim to show that the angle relations imposed by the construction of \mathcal{T}' are the same as the relations present in \mathcal{T} .

From Figure 19 we get immediately:

1. $\nu' = \varepsilon = 2\theta$,
2. $\varepsilon' = \gamma' = \nu = 2\theta$,
3. $\iota' = \lambda = 4\theta$,
4. $\lambda' = \varepsilon + \gamma = 4\theta$,
5. $\mu' = \rho'$, and
6. $\alpha' = \eta'$

The circle in the upper left of corona 1 in Figure 19 shows that $\delta' + \eta' + \tau' = 10\theta$. The circle on the upper left of corona 3 shows that $\alpha' + \kappa' + \mu' = 10\theta$. The circle in the lower right of corona 5 shows that $\chi' + \rho' + \omega' = 10\theta$. Now we turn our attention to the lower right of corona 1. The larger of the two arcs marks angle β' and the smaller marks angle σ' . Recall from the labeling in Figure 7 that $\lambda = 4\theta$ and $\nu = 2\theta$. From these we get $\beta' + \sigma' = \lambda + \nu = 6\theta$.

This gives us angle restrictions

1. $\varepsilon = \gamma' = \nu' = 2\theta$
2. $\iota' = \lambda' = 4\theta$
3. $\beta' + \sigma' = 6\theta$
4. $\gamma' + \rho' + \omega' = 10\theta$

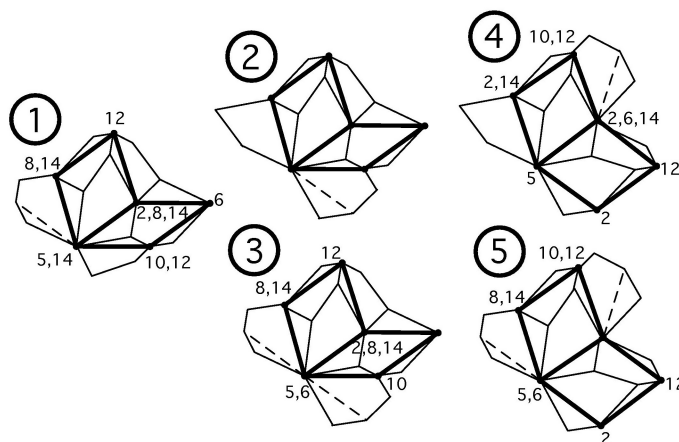


Figure 20: The Ammann coronas with associated Penrose rhombs.

$$5. \delta' + \tau' + \eta' = 10\theta$$

$$6. \alpha' + \kappa' + \mu' = 10\theta$$

$$7. \alpha' = \eta'$$

$$8. \mu' = \rho'.$$

These are exactly the same angle relations of Proposition 4.3 required of an Ammann tiling. Therefore, \mathcal{T}' is an Ammann tiling in the sense of Definition 4.4. \square

Theorem 5.5. *Given an Ammann tiling \mathcal{T} , let \mathcal{P} be its underlying Penrose tiling. Let \mathcal{T}' be the iterated Ammann tiling, let \mathcal{R} be the underlying Penrose tiling of \mathcal{T}' , and let \mathcal{P}' be the tiling produced by applying Penrose composition to \mathcal{P} . Then $\mathcal{P}' = \mathcal{R}$.*

Proof. First, note that \mathcal{R} is well defined by Theorem 4.5. Next, consider the relationship between \mathcal{T} and \mathcal{P} . As discussed in the proof of Proposition 4.2, the way the edges of the tiles in \mathcal{P} cut the tiles of \mathcal{T} is the same within each equivalence class of tile types, meaning that, for example, all type A tiles are cut in exactly the same way. (These cuts are shown in Figure 6.)

Since \mathcal{T}' is an Ammann tiling with corresponding Penrose tiling \mathcal{R} , the edges of \mathcal{R} will cut the tiles of \mathcal{T}' in the same way. To show that $\mathcal{P}' = \mathcal{R}$, it is sufficient to show that the edges of \mathcal{P}' make exactly the same cuts in the tiles of \mathcal{T}' as \mathcal{R} .

Figure 21 shows the five Ammann coronas of \mathcal{T} in the context of all possible second coronas of the Ammann A tiles. The Penrose rhombs of \mathcal{P}' are superimposed. Iterating, we see in Figures 22 and 23 that the tiles of \mathcal{T}' are cut in same way by the edges of \mathcal{P}' as they are by the edges of \mathcal{R} . Therefore, $\mathcal{P}' = \mathcal{R}$. \square

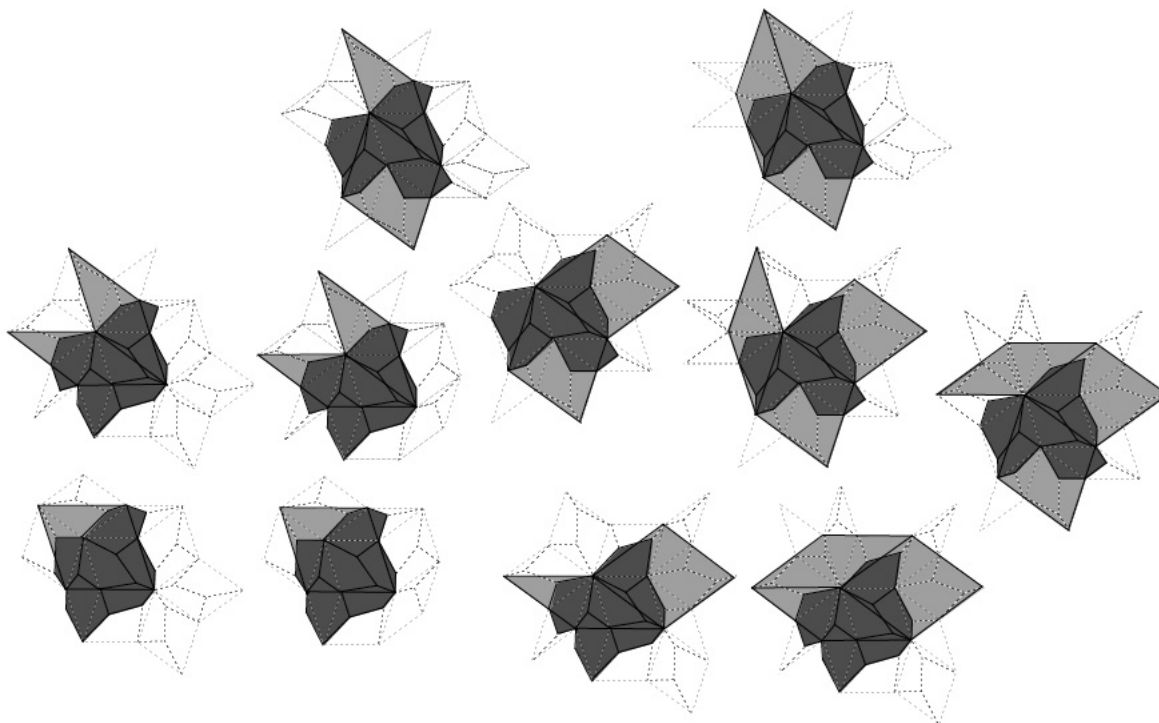


Figure 21: The Ammann coronas with Penrose rhombs of \mathcal{P}' .

Since \mathcal{T}' is an Ammann tiling, iteration may be performed on \mathcal{T}' etc., yielding an infinite sequence of Ammann tilings corresponding to the infinite sequence of underlying Penrose tilings determined by Penrose composition.

6 Dynamics of the Ammann Iteration Process

The Ammann iteration process does not preserve the exact shapes of the prototiles, making it difficult to compare Ammann tilings obtained through repeated iteration. On the other hand, Penrose tiles under composition are easily described, as they are geometrically similar to the original tiles. Thus, appealing to Theorem 5.5, Ammann iteration may be tracked by simultaneously tracking the change in the underlying Penrose tiling and the change in the relative location of the added vertex Q within the Penrose thin rhombs. Recall that the Penrose composition process scales the prototiles by a factor of ϕ , so by rescaling both the Penrose and Ammann tilings by $\frac{1}{\phi}$ after each Ammann iteration, the dimensions of the tiles of the underlying Penrose tiling remain constant throughout, allowing us to quantitatively compare the location of Q within the thin rhomb at each stage of repeated iteration. (A similar method of adjusting length scales is used in [5].)

Since each Ammann iteration reverses the direction of the labeling of the Ammann prototiles, the location of Q_n will alternate between the lower right and lower left quadrants

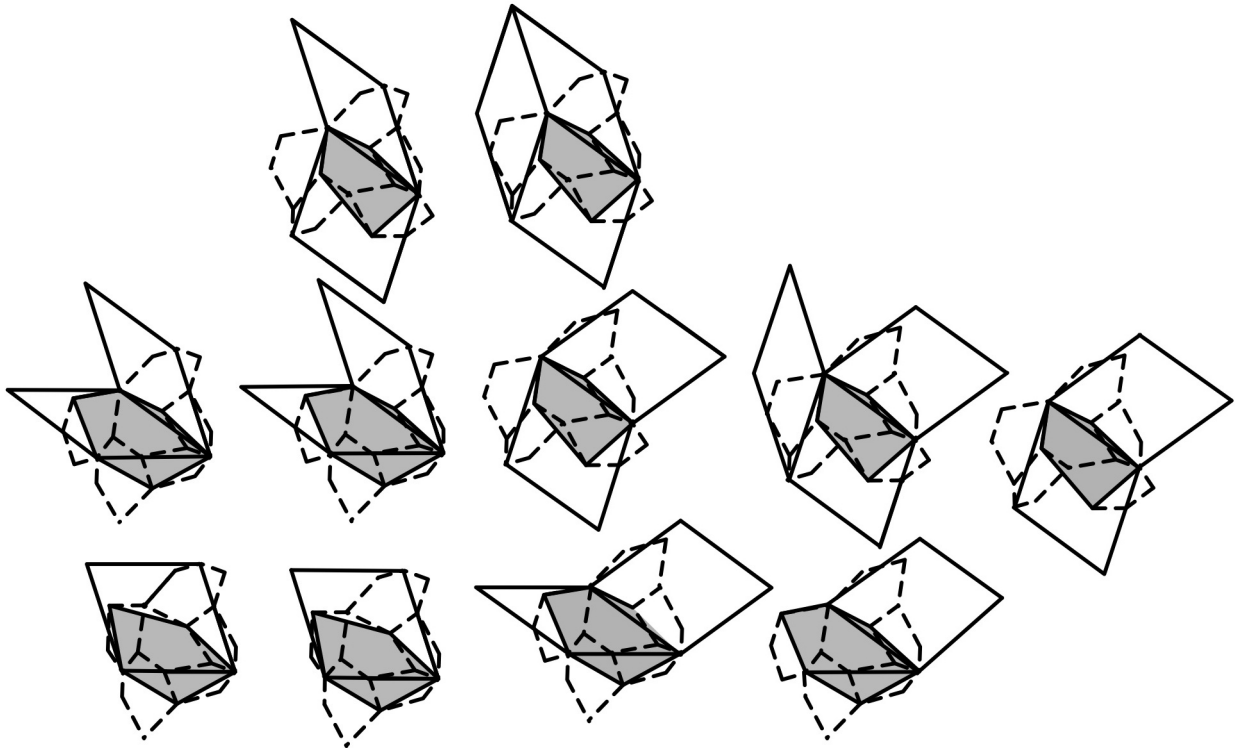


Figure 22: The same coronas as Figure 21 but with the tiles of \mathcal{T}' drawn in.

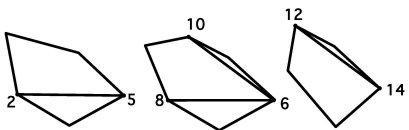


Figure 23: The tiles of \mathcal{T}' with the cuts made by \mathcal{P}' .

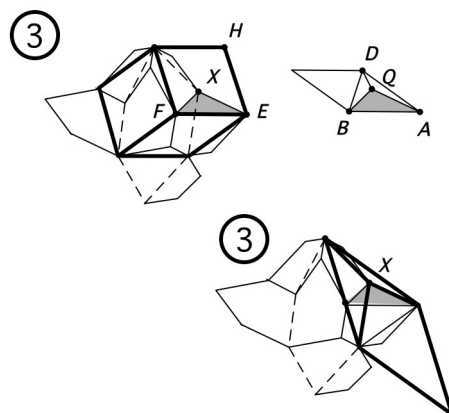


Figure 24:

of the reference thin Penrose rhomb. In order to simplify our analysis, we let the sequence $\{Q_0, Q_1, Q_2, \dots, Q_n, \dots\}$ represent the movement of Q under repeated iteration, but with the odd elements of the sequence reflected through the principal (long) axis of the reference thin rhomb. We locate Q within a Penrose thin rhomb using polar coordinates based along one edge of the rhomb. Accordingly, we locate Q_n by the parameters r_n, θ_n .

Since we will first examine what happens to Q under one application of the iteration process, we denote $Q' := Q_1$. Consider the point denoted X in Figure 24. In the original Penrose tiling, this point lies in a thick rhomb and plays the role of R based on the labeling in Figure 3. Since $\triangle EFR$ is congruent to $\triangle ABQ$, we can equivalently think of X as playing the role of Q in a thin rhomb. The angle measurements of the rhombs ensure that such a thin rhomb lined up in this way would have one edge along the midline of the original thick rhomb, as seen in Figures 24 and 25. On the other hand, performing Penrose composition, we see that X also plays the role of Q' , so we can establish a precise geometric relationship between the location of Q in the original tiling and Q' in the iterated tiling. (See Figure 25.)

Using the law of cosines on the bold triangle in Figure 25, we get:

$$p^2 = r^2 + \phi^2 - 2r\phi \cos \theta.$$

Normalizing, so that $\frac{p}{\phi} = r'$, we arrive at the formula

$$r' = \frac{\sqrt{r^2 + \phi^2 - 2r\phi \cos \theta}}{\phi}. \tag{1}$$

Again, we using the law of cosines on the triangle in Figure 25,

$$\begin{aligned} r^2 &= \phi^2 + p^2 - 2p\phi \cos \theta' \\ &= \phi^2 + (r')^2\phi^2 - 2\phi^2r' \cos \theta'. \end{aligned}$$

Rearranging we have

$$\cos \theta' = \left(\frac{\phi^2 + (r')^2\phi^2 - r^2}{2\phi^2r'} \right),$$

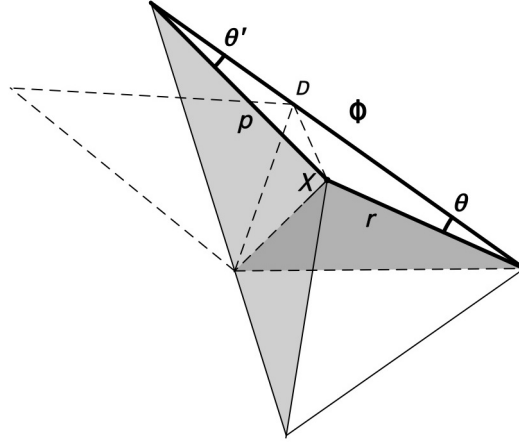


Figure 25: The enlarged triangle from corona 3, Figure 24. Notice that X is located within the dashed half rhomb by (r, θ) and within the solid half rhomb by (p, θ') .

and substituting for r' using 1, we have

$$\cos \theta' = \frac{\phi^2 + \frac{(\sqrt{r^2 + \phi^2 - 2r\phi \cos \theta})^2 \phi^2 - r^2}{\phi}}{2\phi^2 \frac{\sqrt{r^2 + \phi^2 - 2r\phi \cos \theta}}{\phi}},$$

which simplifies to

$$\cos \theta' = \frac{\phi - r \cos \theta}{\sqrt{r^2 + \phi^2 - 2r\phi \cos \theta}}. \quad (2)$$

Thus, the movement of Q is described by the assignment $(r, \theta) \mapsto (r', \theta')$ where

$$(r', \theta') = \left(\frac{\sqrt{r^2 + \phi^2 - 2r\phi \cos \theta}}{\phi}, \arccos \left(\frac{\phi - r \cos \theta}{\sqrt{r^2 + \phi^2 - 2r\phi \cos \theta}} \right) \right). \quad (3)$$

Theorem 6.1. *The map $(r, \theta) \mapsto (r', \theta')$ in 3 has a unique attractive fixed point at $(r, \theta) = (\frac{1}{\phi}, 0)$. (See Figure 26.)*

Proof. Changing to cartesian coordinates,

$$x' = r' \cos \theta' = \left(\frac{\sqrt{x^2 + y^2 + \phi^2 - 2x\phi}}{\phi} \right) \left(\frac{\phi - x}{\sqrt{x^2 + y^2 + \phi^2 - 2x\phi}} \right) = 1 - \frac{x}{\phi}$$

and

$$\begin{aligned} y' &= r' \sin \theta' \\ &= \frac{\sqrt{x^2 + y^2 + \phi^2 - 2x\phi}}{\phi} \sin \arccos \left(\frac{\phi - x}{\sqrt{x^2 + y^2 + \phi^2 - 2x\phi}} \right). \end{aligned}$$

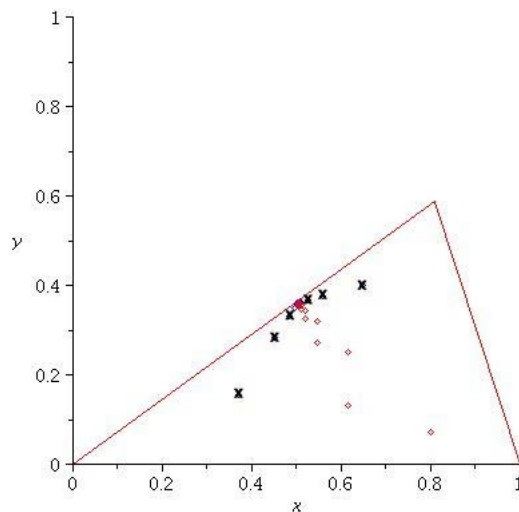


Figure 26: Two different sequences $\{Q_1, Q_2, \dots\}$ denoted by dots and x's corresponding to repeated Ammann iteration shown inside a reference half-rhomb. The sequences both converge to the fixed point specified in Theorem 6.1.

Using the identity $\sin \arccos x = \sqrt{1 - x^2}$, this simplifies to

$$\begin{aligned} y' &= \frac{\sqrt{x^2 + y^2 + \phi^2 - 2x\phi}}{\phi} \left(\sqrt{1 - \frac{(\phi^2 - x\phi)^2}{\phi^2(x^2 + y^2 + \phi^2 - 2x\phi)}} \right) \\ &= \frac{\sqrt{\phi^2(x^2 + y^2 + \phi^2 - 2x\phi) - (\phi^4 - 2x\phi^3 + x^2\phi^2)}}{\phi^2} \\ &= \frac{|y|}{\phi}. \end{aligned}$$

Since we are only interested in positive values of y since $0 \leq \theta \leq \frac{\pi}{5}$, we simply write

$$y' = \frac{y}{\phi}. \quad (4)$$

One more change of variables transforms this affine map to a linear map. Let

$$u = x - \frac{1}{\phi} \text{ and } v = y.$$

Then

$$u' = -\frac{u}{\phi} \text{ and } v' = \frac{v}{\phi}. \quad (5)$$

This is a linear map which fixes $(u, v) = (0, 0)$ and no other point. Going back to the previous coordinate system we have that the map fixes $(x, y) = (\frac{1}{\phi}, 0)$, which is equivalent to the point $(r, \theta) = (\frac{1}{\phi}, 0)$. Furthermore, since $0 < \frac{1}{\phi} < 1$, the eigenvalues for (5) have absolute value less than 1, so the fixed point is attractive. \square

As a final remark, we reiterate what this result does and does not imply. This result proves that Q approaches a limit under repeated iteration, but it is not true in general that the entire tiling approaches a limit, since Penrose composition is a chaotic map in the space of Penrose tilings. As Q approaches its limit, Ammann iteration produces limiting shapes for the prototiles, and these limiting shapes are obtained when Q lies at the point that divides an edge of the thin Penrose rhomb by the golden ratio. The resulting tilings (the most visually appealing of the Ammann tilings) have three pentagonal prototiles, but as noted immediately following 4.1, we still consider one of them as a hexagon (with two of its sides meeting at an angle of π) in order to abide by the standard tiling rule that adjacent tiles must share a complete edge. With this, the limiting tilings are still Ammann tilings by the definition above. A patch of an Ammann tiling admitted by the limiting prototiles is shown in Figure 1.

References

- [1] Ammann, Robert, Branko Grünbaum, and G.C. Shephard. Aperiodic Tiles. *Discrete and Computational Geometry*, 8:1-25, 1992.
- [2] deBruijn, N.G. Algebraic Theory of Penrose's Non-periodic Tilings of the Plane 1. Proceedings of the Koninklijke Nederlandse Akademie Van Wetenschappen Series A-mathematical Sciences, 1981.
- [3] Grünbaum, Branko and G.C. Shephard. *Tilings and Patterns*. W.H. Freeman and Company, New York, 1987.
- [4] Lunnon, W.F. and P.A.B. Pleasants. Quasicrystallographic tilings. *Journal De Mathematiques Pure et Appliquees*, Vol 66. Cauthier-Villars, 1987.
- [5] Priebe, N. and B. Solomyak. Characterization of Planar Psuedo-Self-Similar Tilings. *Discrete and Computational Geometry*, 26:289-306 (2001).
- [6] Priebe, N. Towards a Characterization of Self-similar Tilings in Terms of Derived Voronoi Tessellations. *Geometriae Dedicata*, 79:239-265, 2000.
- [7] Senechal, Marjorie. *Quasicrystals and Geometry*. Cambridge University Press, New York, 1995.
- [8] Solomyak, Boris (1997). Dynamics of self-similar tilings. *Ergodic Theory and Dynamical Systems*, 17, pp 695-738.
- [9] Solomyak, B. Nonperiodicity Implies Unique Composition for Self-Similar Translationally Finite Tilings. *Discrete and Computational Geometry*, 20:265-279, 1998.